THE JOURNAL OF PHYSICAL CHEMISTRY B

Article

pubs.acs.org/JPCB

Oxidation and Nitration of Tyrosine by Ozone and Nitrogen Dioxide: Reaction Mechanisms and Biological and Atmospheric Implications

L. Sandhiya, P. Kolandaivel, and K. Senthilkumar*

Department of Physics, Bharathiar University, Coimbatore 641 046, India

Supporting Information

ABSTRACT: The nitration of tyrosine by atmospheric oxidants, O_3 and NO_2, is an important cause for the spread of allergenic diseases. In the present study, the mechanism and pathways for the reaction of tyrosine with the atmospheric oxidants O_3 and NO_2 are studied using DFT-M06-2X, B3LYP, and B3LYP-D methods with the 6-311+G-(d,p) basis set. The energy barrier for the initial oxidation reactions is also calculated at the CCSD(T)/6-31+G(d,p) level of theory. The reaction is studied in gas, aqueous, and lipid media. The initial oxidation of tyrosine by O_3 proceeds by H atom abstraction and addition reactions and leads to the formation of six different intermediates. The subsequent nitration reaction is studied for all the intermediates, and the results show that the nitration affects both the side chain and the aromatic ring of tyrosine. The rate constant of the favorable oxidation and nitration reaction is calculated using variational transition state theory over the temperature range of 278−350 K. The spectral properties of the oxidation and nitration products are calculated at the TD-M06-2X/6-311+G(d,p) level of theory. The fate of the tyrosine radical intermediate is studied by its reaction with glutathione antioxidant. This study provides an enhanced understanding of the oxidation and nitration of tyrosine by O_3 and NO_2 in the context of improving the air quality and reducing the allergic diseases.

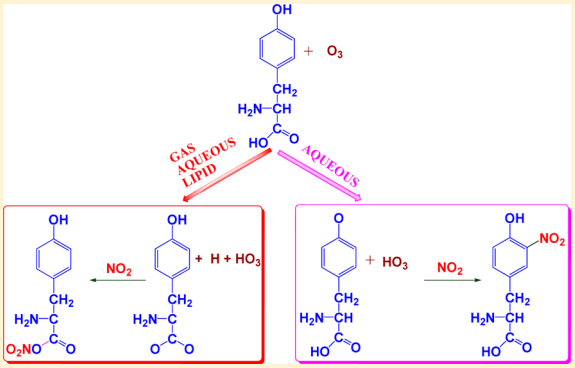

INTRODUCTION

Airborne particles in the atmosphere play a major role in spreading the biological organisms and pathogens and inducing several respiratory, neurological, and allergic diseases.[1−5] The pollen-induced respiratory allergy is related with the presence of fine air particulate matter and traffic-related air pollution.[3,6] High concentrations of nitrogen dioxide and ozone enhance the allergic diseases.[7,8] Despite their important environmental and biological impacts, the mechanism of the interaction of the air particulate matter and air pollutants is least understood. The most prominent group of pollen allergens present in pollen grains is protein molecules, which account for up to 5% of urban air particulate matter.[3] The protein molecules promote allergies when they are nitrated by polluted air before the inhalation and deposition in the human respiratory tract. In particular, the nitration is caused by the interaction of protein molecules with traffic-related air pollutants such as O_3 and NO_2. At elevated concentrations of O_3 and NO_2, the nitration leads to the conversion of the natural aromatic amino acid tyrosine into nitrotyrosine. The conjugates of proteins with these nitroaromatic compounds evade immune tolerance and boost immune responses and therefore enhance the allergenicity of proteins.[9] The important atmospheric oxidant O_3 potentially causes damage to peptides lining on the respiratory tract, thereby causing pollution derived diseases. Another risk assessment associated with the nitration of tyrosine is the formation of tyrosine radical which is usually the reactive oxygen species (ROS). The overall balance between formation and scavenging of ROS and free radicals in the body results in the so-called oxidative stress.[10] This oxidative stress increases the risk of lung cancer.[11] Moreover, the nitration of protein tyrosine residues to nitrotyrosine induces the disruption of nitric oxide signaling and metabolism related to the pro-oxidant process, a condition called nitrooxidative stress.[12] Depending upon the heterogeneity of the environment around the tyrosine residues within a protein, the nitration efficiencies could vary from one residue to another.[13] The spread of these diseases can be counteracted by improving the air quality, which is achieved by understanding the atmospheric chemistry behind the nitration process.

Among the protein molecules, approximately 1−10 residues of tyrosine per 100 000 proteins are found to be nitrated under inflammatory conditions.[14] All cellular proteins are having important tyrosine residues. The tyrosine possesses relatively large phenolic amphipathic side chain and is capable of interacting with the oxidants when exposed in the atmosphere. Previous studies show that the nitration of tyrosine is a two-step process.[14,15] The first step is the oxidation of the phenolic site of tyrosine (Tyr) (see Figure 1) to a one-electron oxidation product, Tyr radical. In the second step, NO_2 is added to the

Received: September 4, 2013
Revised: March 11, 2014
Published: March 11, 2014

dx.doi.org/10.1021/jp4106037 | J. Phys. Chem. B 2014, 118, 3479−3490

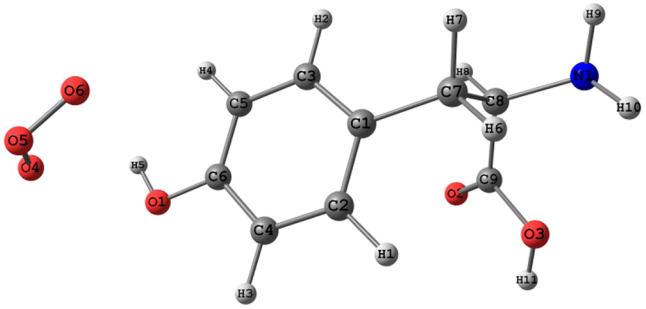

Figure 1. Optimized structure of the tyrosine + O_3 reaction system.

Tyr radical in radical−radical termination reaction. The nitrotyrosine is also formed in an alternative pathway due to the reaction between tyrosine and NO in a two-electron oxidation process.[14] The aqueous or hydrophobic environment can also influence the mechanism of nitration and dimerization of tyrosine.[16] The nitration process is kinetically favored over the dimerization process, but both the processes occur simultaneously, resulting in the aggregation of cross-linked proteins in tissues leading to degenerative disease conditions and the aging process.[14] Recently, the mechanism of protein tyrosine nitration in lipid-rich biostructures has been accessed by Bartegashi et al.[17] Their study revealed that the nitration of tyrosine could occur inside the lipid bilayer during the lipid perooxidation reactions. A recent study showed that the principal oxidation of tyrosine is initiated by O_3 and then followed by the addition of NO_2, leading to the formation of nitrotyrosine.[18] But, there are many reactive sites in tyrosine other than the phenolic site in which the oxidation can take place. The reaction of the initially formed Tyr radical with NO_2 is a diffusion-controlled process[19,20] and can lead to the formation of nitrotyrosine. However, the competing reactions are expected to be fast, leading to other Tyr radical derived products. In the atmosphere, the reaction between chemical compounds and O_3 usually proceeds by the H atom abstraction reactions or addition reactions. Hence, many reaction pathways are possible for the initial oxidation of tyrosine by O_3. But, the actual reaction mechanism and pathways leading to the nitration of tyrosine in the atmosphere are less understood. The careful examination of the possibility of the reaction pathways is essential to control nitration-related diseases.

The oxidation of tyrosine is controlled by antioxidants present in living organisms. Glutathione is recognized as an important endogenous low-molecular-weight antioxidant and is an important constituent in the respiratory tract lining fluid.[21] During oxidative stress, the level of glutathione is depleted, which results in the lowering of ability of living organisms to resist further stress. The radicals formed in the initial oxidation are immediately repaired by the reaction with glutathione, and the glutathione thiyl radical is formed along with the regenerated tyrosine.[22] Several studies have focused on the reaction of glutathione with tyrosyl radical.[23] But, the other radicals formed in the initial oxidation are also responsible for the sink of glutathione. In order to understand the biological implications of the oxidation and nitration of tyrosine, the subsequent radical sink hypothesis of glutathione is vital. This can be achieved by identifying all possible radicals formed in the initial oxidation and their feasibility to undergo reaction with glutathione. Although the chemistry of O_3 and NO_2 in the atmosphere is well-known, the role of these oxidants on the oxidative damage in biomolecules is least understood.

In view of the above-mentioned exposures, in the present investigation, we made an attempt to model the reaction mechanism and identify the atmospheric reaction pathways for the nitration of tyrosine by O_3 and NO_2 by using quantum chemical methods. By exploring the energies and geometries of the intermediates and transition states on the PES of the reaction system, the minimum-energy reaction paths for the product channels are identified. Existing evidence reveals that the mechanism of tyrosine nitration in biological systems is mediated by free radical reactions in which Tyr radical is formed as an intermediate and subsequently react with either NO or NO_2.[15] Similarly, in the atmosphere, the nitration of tyrosine is initiated by reaction with O_3 and subsequent reaction with NO_2. The nitration of tyrosine can take place through two different mechanistic scenarios. One of the mechanisms involves H atom abstraction from different reactive sites of tyrosine by O_3, and the other mechanism involves the addition of O_3 to the aromatic ring and side chain of tyrosine, both mechanisms followed by reaction with NO_2. Thus, the tyrosine acts as a sink for atmospheric oxidants. The tyrosine oxidation and nitration depend on the environment where the tyrosine residues are present. In order to incorporate the environmental effect on nitration, the reactions are studied in gas, aqueous, and lipid phases. Because of the high concentration of the unsaturated fatty acids in lipidic milieu, the reaction of tyrosine oxidation products with the key antioxidant glutathione is found to be less favorable in lipid medium than in aqueous medium.[23] Hence, the reaction between the radicals formed in the initial oxidation and glutathione is studied in all the three phases to understand this context. The geometries and electronic structures as well as the energy barriers provide the basis for the qualitative analysis of the factors responsible for tyrosine nitration. The kinetic parameters such as rate constant and apparent activation energy, which represent an average over the barriers of the underlying microscopic processes, are calculated using variational transition state theory. The theoretical results obtained from this study may also provide a general understanding of the prevailing uncertainty in the nitration of tyrosine.

COMPUTATIONAL METHODS

The geometries of the reactants, intermediates, transition states, and products on the ground state potential energy surface (PES) of the reaction system are optimized using the hybrid meta exchange-correlation functional M06-2X with 6-31G(d,p) and 6-311+G(d,p) basis sets. The M06-2X functional, which is based on simultaneously optimized exchange and correlation contributions both including kinetic energy density, has been shown to perform excellently in main-group thermochemistry and kinetics for a variety of benchmark sets.[24−28] The solvent effects of the reactive species are studied with geometry optimization at the M06-2X/6-311+G(d,p) level of theory in conjunction with the SMD continuum model.[29] The solvents used are pentyl ethanoate and water to mimic lipid and aqueous environments. The dielectric constant of pentyl ethanoate is 4.73, and that of water is 78.35. The SMD model is a universal solvation model which includes two components: (1) the bulk electrostatic contribution that results from the self-consistent reaction field treatment and (2) the contribution that arises from short-range interactions between the solute and solvent molecules in the first solvation shell. Recent studies have shown that the SMD model is accurate enough to describe the energetics in solvent and is computationally less demanding

dx.doi.org/10.1021/jp4106037 | J. Phys. Chem. B 2014, 118, 3479−3490

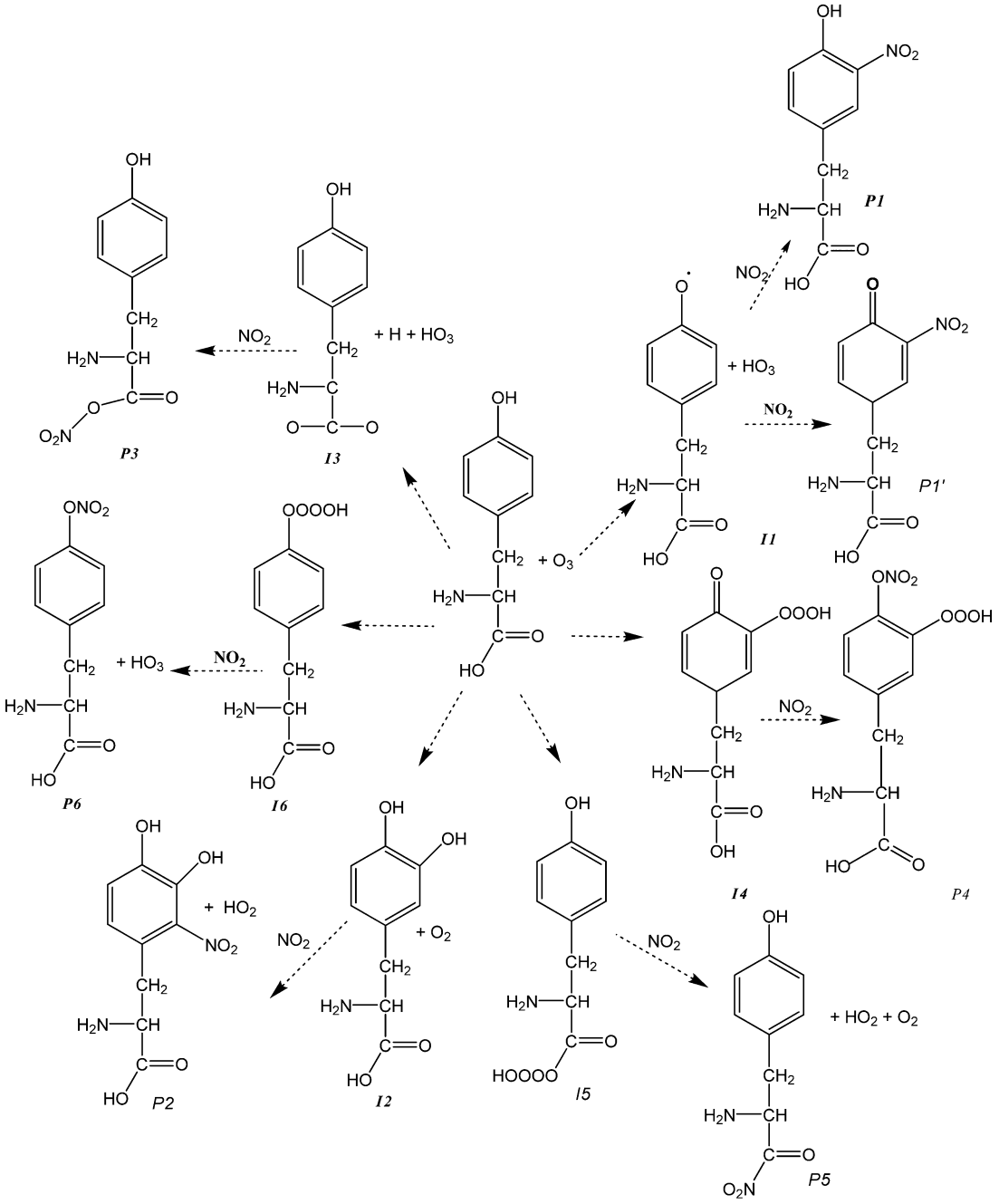

Figure 2. Proposed reaction scheme for the initial oxidation and subsequent nitration reactions of tyrosine.

than the other continuum models.[30,31] Harmonic vibrational frequency calculations were performed at the M06-2X/6-311+G(d,p) level of theory to verify the nature of the stationary points. All minima were confirmed with all positive frequencies, and each transition state had one imaginary frequency confirming its maxima in one reaction coordinate. The connectivity of the transition states with their designated reactants and products was verified in each case by performing intrinsic reaction coordinate (IRC) calculations at the same level of theory. The solvent phase free energy of activation is determined by calculating the free energy change associated with medium change from a gas phase at 1 atm pressure to a solvent phase concentration of 1 M. An energy correction of 1.89 kcal/mol is used to calculate the energy change from gas to solution phase. The solvent cage effect in free energy calculation is accounted by means of free volume theory,[32] and the correction of 2.96 kcal/mol decrease in free energy is used as proposed by Okuno.[33] The M06-2X calculations were performed using an ultrafine integration grid. Since, a recent study[34] has shown that the M06-2X functional is able to reproduce the results obtained at CCSD(T) calculations with sufficient accuracy for all the stationary points on the ground state PES, electron correlation was accounted by performing single-point energy calculations at the coupled cluster method with single and double substitutions with noniterative triple excitations, CCSD(T)[35] using 6-31+G(d,p) basis set with the geometries optimized at the M06-2X/6-311+G(d,p) level of theory. For comparison purposes, the computations were also carried out using B3LYP[36] and B3LYP-D[37,38] methods with the 6-311+G(d,p) level of theory. Further, the spectral properties

dx.doi.org/10.1021/jp4106037 | J. Phys. Chem. B 2014, 118, 3479−3490

of the oxidation and nitrated products are studied using time-dependent density functional theory (TDDFT) at the M06-2X/6-311+G(d,p) level of theory, in order to access the effect of oxidation and nitration upon exposure of UV light.[39] The CD spectra were calculated from the excited state calculation of the favorable reactive species using the TDDFT method. The lowest ten singlet excited states were calculated with their respective wavelength and rotational strengths. The CD spectra were simulated by overlapping Gaussian functions for each transition according to the relation[40]

$$\Delta\varepsilon(E) = \frac{1}{2.297 \times 10^{-39}} \frac{1}{\sqrt{2\pi\sigma}} \sum_{i}^{A} \Delta E_i R_i e^{[-E-\Delta E_i/2\sigma]^2} \quad (1)$$

where σ is the width of the band and ΔE_i and R_i are the excitation energies and rotatory strengths for transition, i, respectively. Rotatory strength determines the intensity of the absorption band, and for transition between states $|\psi_0\rangle$ and $|\psi_i\rangle$, the rotatory strength is defined as

$$R_{0i} = \mathrm{Im}(\langle\psi_0|\hat{\mu}|\psi_i\rangle\langle\psi_0|\hat{m}|\psi_i\rangle)$$

$$R_{0i} = |\vec{\mu}_{0i}|\cdot|\vec{m}_{0i}|\cdot\cos(\vec{\mu}_{0i}, \vec{m}_{0i}) \quad (2)$$

All the electronic structure calculations were performed using the Gaussian 09 program package.[41]

The computed potential energy surface and associated transition state parameters were directly utilized to predict the rate constant as a function of temperature in both gas and solvent phases. The theoretical rate constants for the reactions are calculated using canonical variational transition state theory (CVT), from which the rate constant is given by the formula

$$k^{\mathrm{CVT}}(T) = \min_R k^{\mathrm{GT}}(T, s) \quad (3)$$

where

$$k_c^{\mathrm{GT}}(T, s) = \frac{\sigma k_B T}{\beta h} \frac{Q_c^{\mathrm{GT}}(T, s)}{\varphi_c^R(T)} \exp[-\beta V_{\mathrm{MEP}}(s)] \quad (4)$$

where $k^{\mathrm{GT}}(T,s)$ is the generalized transition state theory rate constant, σ is the symmetry factor accounting for the possibility of more than one symmetry related reaction path, $Q_c^{\mathrm{GT}}(T,s)$ is the classical partition function for the generalized transition state dividing surface, $\phi_c^R(T)$ is the reactant partition function per unit volume, $V_{\mathrm{MEP}}(s)$ is the classical potential energy at point s on the minimum-energy path, k_B is Boltzmann's constant, and h is Planck's constant. The quantity $(\beta h)^{-1}$ is called the universal transition state frequency factor.

Since the CVT rate constant neglects the tunneling, it underestimates the rate constant for the reactions in which quantum tunneling is predominant, especially at low temperatures. Hence, in order to account for the dynamical quantum effects of reaction-coordinate tunneling, a multiplicative transmission coefficient $\kappa(T)$ is used in eq 3 as

$$k_c^{\mathrm{CVT}}(T) = \kappa(T) k^{\mathrm{CVT}}(T) \quad (5)$$

The transmission coefficient $\kappa(T)$ corresponding to tunneling is evaluated by the small-curvature approximation to the vibrational adiabatic potential energy surface. In this approximation, the tunneling is assumed to occur along a multidimensional minimum-energy path. The potential energy curve is approximated by a contracted adiabatic energy barrier which goes through the ZPVE corrected energy of the reactants, transition states, and products. The kinetic calculations are carried out using the GAUSSRATE 2009A[42] program which is an interface program between GAUSSIAN 09 and POLYRATE 2010A programs.[43]

RESULTS AND DISCUSSION

Reaction Mechanism and Reaction Pathways. The optimized structure of the tyrosine + O_3 reaction system is shown in Figure 1. The proposed reaction scheme for the nitration of tyrosine by O_3 and NO_2 is shown in Figure 2. The reactive species are optimized at the M06-2X level of theory with 6-31G(d,p) and 6-311+G(d,p) basis sets and also at B3LYP and B3LYP/D methods with the 6-311+G(d,p) basis set. The average root-mean-square deviation (rmsd) between the internal coordinates of the structures obtained for the initial H atom abstraction reaction with 6-31G(d,p) and 6-311+G(d,p) basis sets using the M06-2X method is 0.08 Å for the reactant and 0.09 Å for the transition state and the intermediate. The energy barriers calculated at the M06-2X/6-311+G(d,p) level of theory are summarized in Tables 1 and

Table 1. Energy Barrier (in kcal/mol) Calculated for the Intermediates Formed in the Initial Oxidation of Tyrosine by O_3

	M06-2X/6-311+G(d,p)			
reactive species	gas	aqueous	lipid	CCSD(T)/6-31+G(d,p) (gas)
I1	28.1	3.9	25.2	25.7
I2	21.4	3.6	19.3	13.7
I3	2.4	4.2	3.9	3.7
I4	4.4	33.9	32.1	9.5
I5	25.4	128.5	131.2	23.7
I6	16.1	19.8	17.0	16.4

Table 2. Energy Barrier (in kcal/mol) Calculated for the Subsequent Nitration of the Intermediates

	M06-2X/6-311+G(d,p)		
reactive species	gas	aqueous	lipid
P1	11.6	3.5	1.2
P2	21.8	19.3	8.3
P3	14.0	27.8	18.7
P4	4.1	27.5	26.5
P5	74.2	64.3	67.4
P6	34.6	39.2	42.2

2, and the values calculated at the M06-2X/6-31G(d,p) level of theory are summarized in Table S1 of the Supporting Information. As given in Table 1 and Table S1, the energy values obtained with the two basis sets are comparable in most of the cases. These results reveal that the basis set dependence of the reaction pathway is not appreciable in the studied reactions. The average rmsd between the internal coordinates of the structures obtained for the initial H atom abstraction reaction with the M06-2X/6-311+G(d,p) and B3LYP/6-311+G(d,p) level of theories is 0.29, 0.21, and 0.08 Å respectively for the reactant, transition state, and product. The average rmsd between the internal coordinates of the structures obtained for the initial H atom abstraction reaction with the M06-2X/6-311+G(d,p) and B3LYP-D/6-311+G(d,p) level of theories is 0.01 Å for the reactant and 0.05 Å transition

dx.doi.org/10.1021/jp4106037 | J. Phys. Chem. B 2014, 118, 3479−3490

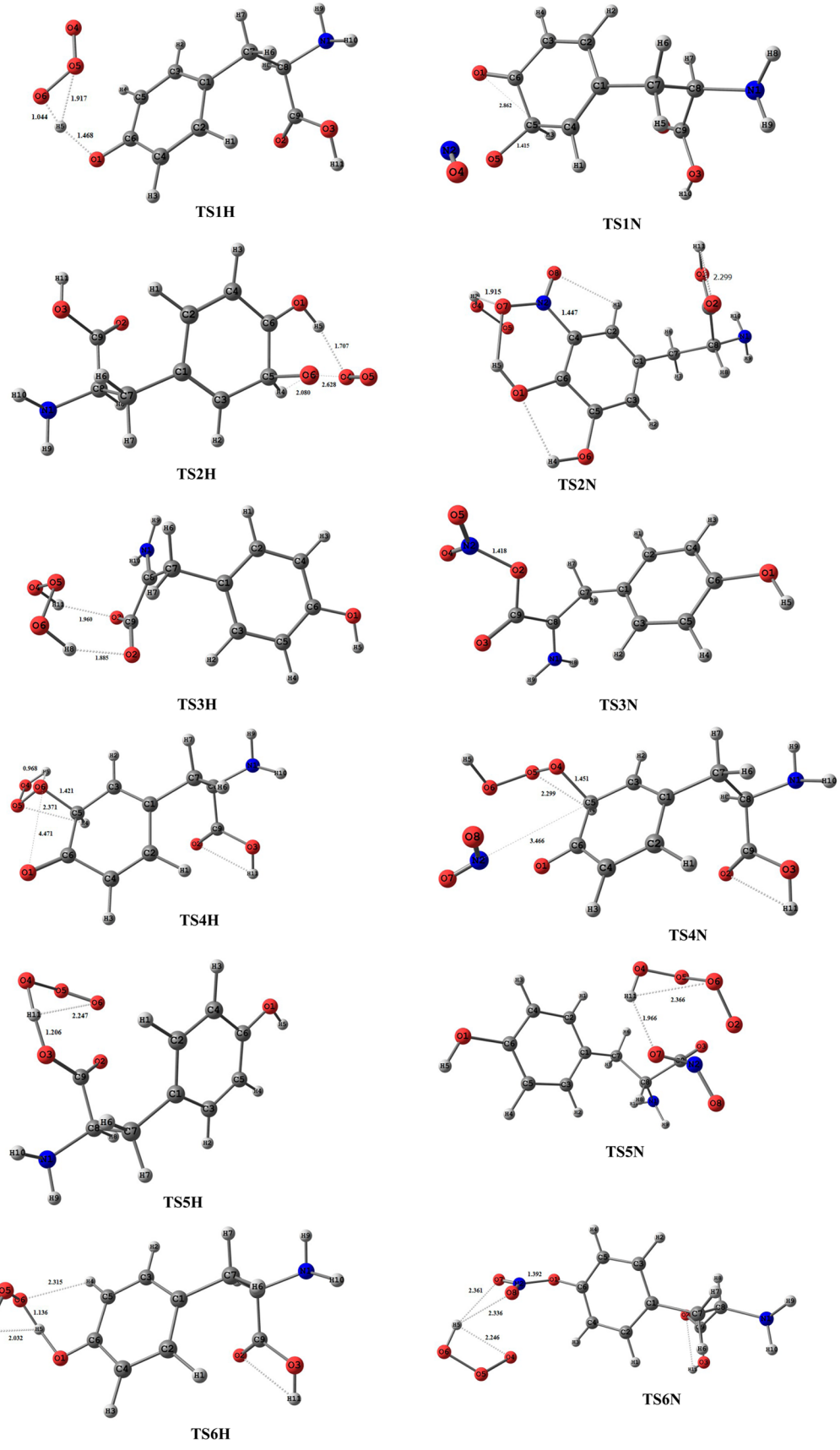

Figure 3. Optimized structure of the transition states involved in the initial oxidation and subsequent nitration of tyrosine by O_3 and NO_2.

state and product. Note that the above-mentioned rmsd includes the interactions of both bonded and nonbonded atoms. The large rmsd is due to the difference in the dihedral angles of the structures calculated using the M06-2X and

dx.doi.org/10.1021/jp4106037 | J. Phys. Chem. B 2014, 118, 3479−3490

B3LYP methods. For instance, in the TS1H structure, the φ(C6−O1−H5−O6) is 1.29° and −2.23° respectively at the M06-2X and B3LYP methods. The energy barriers calculated at the B3LYP and B3LYP-D methods are summarized in Table S2. From Table 1 and Table S2, it is observed that the energy barrier calculated at the B3LYP-D method is comparable with that of the M06-2X method in most of the cases, whereas the results obtained from the B3LYP method deviate from the results obtained at the M06-2X method. Though, the energetics obtained with the three DFT methods vary slightly, the relative importance of the product channels does not change with respect to the methods; i.e., the most favorable reaction channel is the same in all the methods studied. It has been reported in a recent study[44] that the energy barrier calculated using the CCSD(T) method is accurate, and the results obtained from the M06-2X functional are comparable with those obtained from the CCSD(T) method. In agreement with the above study, in the present investigation, the energy barrier calculated at the CCSD(T)/6-31+G(d,p)//M06-2X/6-311+G(d,p) level of theory is comparable with the results obtained from the M06-2X/6-311+G(d,p) level of theory in most of the cases. The error bar of the energetic parameters calculated using the M06-2X and CCSD(T) methods is ∼2 to 8 kcal/mol. An error of 2 kcal/mol in barrier height will lead to an error in calculated rate constant by 1 order of magnitude. Hence, the structure and energetics obtained using the M06-2X functional with the 6-311+G(d,p) basis set are discussed in detail and are used in further kinetic calculations.

As shown in Figure 1, six different principal oxidation steps are possible for the reaction between tyrosine and O_3. The optimized structure of the transition states involved in the oxidation and subsequent nitration is shown in Figure 3. The optimized structure of the intermediates and products is shown in Figure S1. For labeling of atoms, see Figures 1, 3, and S1. The calculated energy barriers for the initial oxidation reactions in gas and solvent media calculated at the M06-2X method are summarized in Table 1 along with the values calculated at the CCSD(T)/6-31+G(d,p)//M06-2X/6-311+G(d,p) level of theory. The relative energy profile of the reaction pathways involved in the initial and subsequent reactions is illustrated in Figure 4. The relatively large phenolic amphipathic side chain of tyrosine supports its ability to interact with water and also to undergo nonpolar interactions.[45] The H atom abstraction from the phenolic site of tyrosine results in the formation of reactive oxygen intermediate (ROI), **I1**, through a transition state, **TS1H**. As reported in a recent study,[10] this ROI is identified as the phenoxy radical derivative of tyrosine (Tyr radical). The transition state, **TS1H**, is a hydrogen-bonded complex in which the H5 atom of phenolic group of tyrosine forms a hydrogen bond with the O6 and O5 atoms of O_3, and the hydrogen bond lengths are 1.044 and 1.917 Å, respectively (see Figure 3). The large energy barrier of 28.1 and 25.2 kcal/mol is calculated for this reaction in gas and lipid media; that is, the formation of ROI is a rate-limiting step, which is consistent with the recent experimental study[18] (see Table 1). But, the energy barrier calculated for this reaction in aqueous medium is only 3.88 kcal/mol, which suggests that the formation of tyrosyl radical is more feasible in aqueous medium.

Earlier studies show that the phenoxy radicals are well determined intermediates in the nitration of phenolic compounds by NO_2.[46,47] Hence, the initial step is followed by the reaction of **I1** with NO_2 in which the H atom attached to C5 atom is transferred to phenolic radical site, and then the

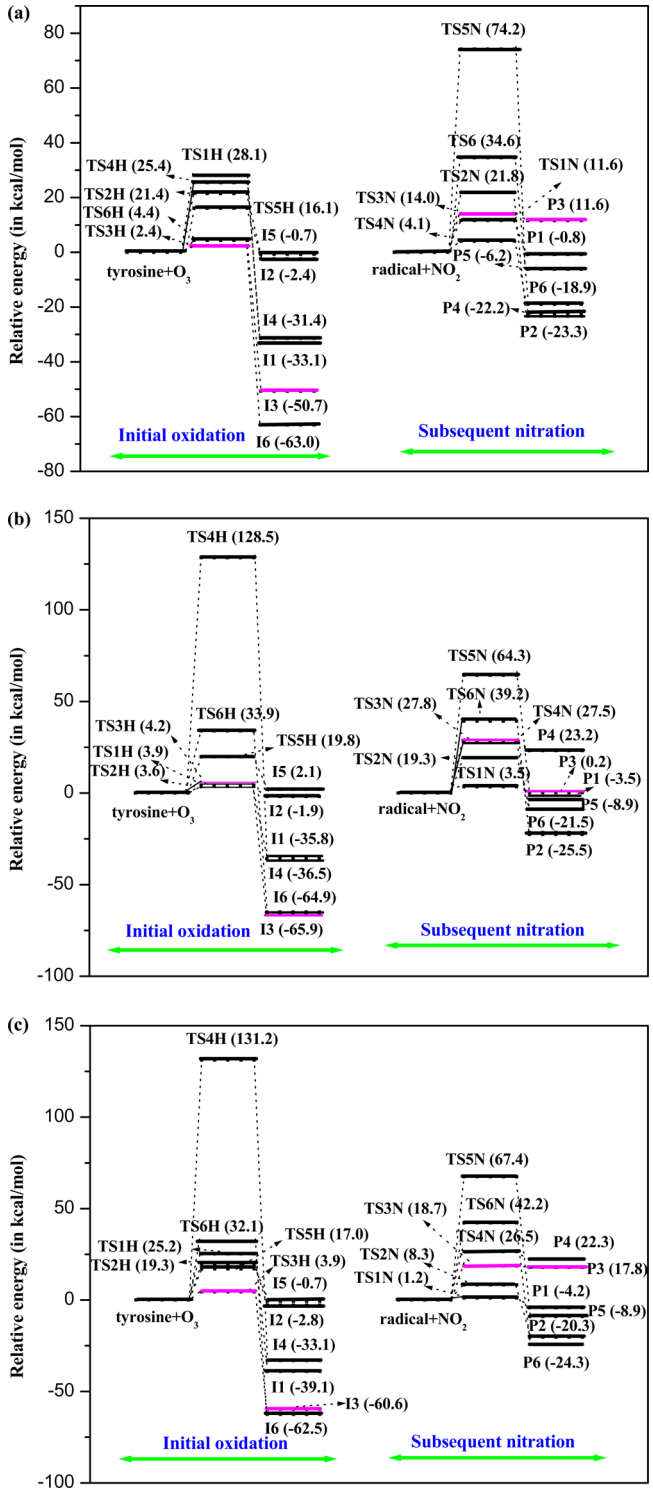

Figure 4. Relative energy profile of the reactive species involved in the initial oxidation and subsequent nitration of tyrosine by O_3 and NO_2 in (a) gas phase, (b) aqueous phase, and (c) lipid phase.

NO_2 group is attached to the C5-radical site, leading to the formation of nitrotyrosine (**P1**) as a product. The bonded nitro group will act as a hydrophobic substituent and will trigger conformational changes. This nitration process is characterized by a transition state, **TS1N**. As given in Table 2, the energy barrier for this nitration process is different for different media. This is partially attributed to the difference in pK_a value of tyrosine and nitrotyrosine.[48] The pK_a value of nitrotyrosine

dx.doi.org/10.1021/jp4106037 | J. Phys. Chem. B 2014, 118, 3479−3490

decreases to about 7.5 from 10 of tyrosine.[49] Table 2 illustrates that the nitration of tyrosine in lipid medium appears to be favorable than the gas and water media. The calculated energy barrier for the formation of **P1** is 11.6, 3.5, and 1.2 kcal/mol respectively in gas, water, and lipid media. This result is in parity with the notion of favorability of the reaction of phenolic compounds in nonpolar solvents.[17] The pentyl ethanoate used to mimic the lipid media acts as a better electron donor and enhances the likelihood of nitration. That is, the nitration of tyrosine strongly depends on the medium. The nitrotyrosine exists in anionic form, and the negatively charged hydrophilic nature promotes the large structural modifications and further reactions with other subunits in the protein.[49] In addition to the formation of nitrotyrosine (**P1**) product channel, the reaction between **I1** and NO_2 may also lead to the formation of another product channel, nitro carbonyl of tyrosine (**P1′**) in which the NO_2 group is attached to the C2-site and C1−O1 bond acquires double-bond character. This nitration reaction occurs through a transition state, **TS1N′**, with an energy barrier of 12.7, 10.5, and 7.4 kcal/mol in gas, aqueous, and lipid media, respectively. The structure of **P1′** and its corresponding transition state **TS1N′** is shown in Figure S2 of the Supporting Information. The energy barrier calculated for these two product channels suggests that NO_2 is consumed quickly by reacting with **I1**, which is in accordance with the recent experimental study.[18]

It is obvious from earlier studies that the nitrated and cross-linked protein aggregates in tissues[12,14,50] and hence the dimerization of Tyr radical may also be possible under physiologically relevant conditions. In the absence of NO_2, **I1** is stabilized through self-reaction resulting in the formation of tyrosine dimer. The optimized structure of the tyrosine dimer is shown in Figure S3. This dimerization reaction takes place with an energy barrier of 35.6, 21.2, and 78.4 kcal/mol respectively in gas, aqueous, and lipid media. This reaction is favorable in aqueous medium where the diffusion is fast, whereas in the lipid medium the magnitude of diffusion is slower than that in the aqueous medium. This reaction is of biochemical concern which alters the protein assembly and enhances the protein degradation. The results of tyrosyl radical and tyrosine dimer formation show that tyrosyl radical is formed with a faster rate than the dimerization.

The next H atom abstraction reaction takes place at the C5 atom in which the H atom is abstracted by one of the O atoms of O_3 and the newly formed OH group binds with the C5 atom, and the oxygen molecule is eliminated. Thus, in this reaction, 3-hydroxytyrosine is formed as the new intermediate, **I2**. This dihydroxy aromatic molecule was previously observed as an intermediate from the peroxynitrite-initiated oxidation of tyrosine.[51] This reaction occurs via a transition state, **TS2H**, with an energy barrier of 21.4, 3.6, and 19.3 kcal/mol respectively in gas, aqueous, and lipid media. As shown in Figure 3, in the **TS2H** structure, the O6 atom is transferred to C5 atom, and a hydrogen bonding of 1.706 Å exists between the H5 and O4 atoms and the O6−H4 bond length decreases by 0.5 Å from that of the initial reactants. As suggested by the calculated energy barrier, the dihydroxy intermediate is formed rapidly in aqueous medium than in the other media. Even though the dihydroxy intermediate is formed with a small energy barrier in aqueous medium, it is less preferable to act as an intermediate for nitration because of its low reactivity with NO_2.[52] However, in the presence of O_2, which was eliminated in the initial step, the intermediate **I2** can undergo reaction with NO_2. Thus, if sufficient NO_2 and O_2 are present, the electron-rich aromatic ring is likely to undergo hydrogen atom transfer process after the initial hydrogen atom transfer reaction. Thus, NO_2 acts as a strong ortho−para director. Here the H atom bonded with the C atom of **I2** is abstracted by O_2, and NO_2 is attached at the C3-radical site of **I2**, resulting in the formation of **P2** product channel. This reaction is associated with a transition state **TS2N**, with an energy barrier of 21.8, 19.7, and 24.4 kcal/mol in gas, aqueous, and lipid phases, respectively. As shown in Figure 3, the distance between the N atom of NO_2 and the C3 atom of **I2** is 2.1 Å in **TS2N** which was 3.1 Å in the reactant. Further, the distance between the O atom of O_2 and the H1 atom attached to the C3 atom in **TS2N** decreases by 1 Å from that of the reactant.

The H atom abstraction from the tyrosine by O_3 may lead to the formation of a hydrogen-bonded complex, **I3** (see Figure S1). This complex is formed by the abstraction of two H atoms: one from the phenolic moiety attached to the carbonyl group of tyrosine and the other from the CH group attached to the amine group of tyrosine. The abstracted H atoms form hydrogen bonding with the oxygen atoms attached to the C9 atom. In the intermediate, **I3**, the O3−H11 hydrogen bond distance is 2.112 Å and the H8−O2 hydrogen bond distance is 1.975 Å. As summarized in Table 1, this complex formation is characterized by a transition state, **TS3H**, with a small energy barrier in all the media. Thus, this reaction pathway is kinetically viable. The hydrogen bond distances of O3−H11 and H8−O2 bonds in **TS3H** structure are around 1.822 and 2.135 Å, respectively. The BSSE corrected interaction energy calculated for the **I3** complex is −50.3 kcal/mol, showing the stability of the **I3** complex. The BSSE energy for the **I3** complex is about 6.7 kcal/mol. The stable **I3** complex can react weakly with NO_2 to form a nitrated complex, **P3**. In this case, the nitration occurs in a two-step process. In the presence of NO_2, initially the HO_3 radical is removed from the complex in a barrierless reaction. The second step involves the binding of NO_2 to O2 atom through a transition state **TS3N** with an energy barrier of 14.0, 27.8, and 18.7 kcal/mol respectively in gas, aqueous, and lipid media. The transition state **TS3N** is a late transition state and is product-like. As shown in Figure S1, in **TS3N**, the O2−N2 bond distance increased by 2 Å from that of the reactants and 0.5 Å greater than that of the nitrated complex, **P3**.

Binding of O_3 at C5, C6, and O2 sites of tyrosine leads to the formation of hydroperoxide adducts **I4**, **I5**, and **I6**, respectively (see Figure 2). These hydroperoxides were identified in the photooxidation of free Tyr residues by O_2 followed by decomposition reactions.[53] The interaction of O_3 at C5 and O2 sites abstracts the H atom from the OH group of the corresponding sites, and one of the terminal O atom of O_3 binds with the phenolic radical site. The interaction of O_3 at the C6 site results in the abstraction of H atom from the phenolic moiety attached at the C5 atom and the terminal oxygen atom of O_3 binds with the C6 atom. The C5 atom acquires double bond character with the O1 atom. As shown in Figure 4, the interaction of O_3 at C5, C6, and O2 sites is associated with the energy barrier of 4.4, 25.4, and 16.1 kcal/mol respectively at transition states **TS4H**, **TS5H**, and **TS6H** in the gas phase. The formation of **I5** adduct takes place with a large energy barrier of 128.5 and 131.2 kcal/mol in aqueous and lipid media, whereas the **I4** and **I6** adducts are formed with comparable energy barrier (∼33 kcal/mol in aqueous medium and ∼18 kcal/mol in lipid medium) in the solvent media. The subsequent

dx.doi.org/10.1021/jp4106037 | J. Phys. Chem. B 2014, 118, 3479−3490

nitration reaction of the intermediates **I4** and **I6** leads to the elimination of HO_2 and O_2 from **I4** and **I6** and the addition of NO_2 to C5 and O2-radical sites, resulting in the formation of products **P4** and **P6**, respectively. These nitration reactions at C5 and O2-sites are associated with energy barriers of 21.8 and 74.2 kcal/mol, in gas phase through the transition states, **TS4N** and **TS6N**. The reaction between **I5** and NO_2 results in the formation of HO_3 and the nitrated complex, **P5**. The HO_3 group attached to the C6 atom is eliminated, and NO_2 is added to the C6-radical site. This nitration process is characterized by a transition state, **TS5N**, with a small energy barrier of 4.1 kcal/mol. Among the three adduct complexes, the nitration occurs more favorably with the intermediate, **I4**. This is because the O atom attached at C6-site increases the ring electron density and allows for the addition of electrophilic NO_2 radical. The intermediates **I4**, **I5**, and **I6** can also undergo radical-induced oxidative cyclization of the −OOO− group, resulting in the formation of epoxy radicals. But, the pathways corresponding to this epoxy radical formation are least possible due to less flexible backbone in proteins which prevents the conformational change required for the epoxy formation.[49] These pathways reveal that once the tyrosine is damaged by oxidation, it is more prone to undergo further nitration. From Table 1, it is observed that the intermediates **I1**, **I2**, and **I3** are formed more favorably in water medium, and the formation of intermediate **I3** takes place more feasibly in all the three media studied. In the subsequent nitration reactions, the nitrated product **P1** is formed more favorably in the solvent media, whereas in the gas phase, the formation of product **P4** is more feasible. Also, the formation of nitrated product **P3** is expected on the basis of small energy barrier calculated for **I3**, the oxidation product of tyrosine.

The fate of the radicals formed in the initial oxidation is determined by their reaction with antioxidants present in living organisms. Most commonly, the radicals formed in the initial oxidation reaction likely react with glutathione (GSH), an antioxidant. The reaction between the most favorable intermediate **I3** and GSH is studied. The reaction is a two-step process. In the first step, the H atom in carboxylic acid group of GSH is abstracted by the C-centered radical site of **I3** in a barrierless reaction. In the second step, the reaction proceeds by the H atom abstraction from GSH by the O-radical site of **I3**, leading to the regeneration of tyrosine along with glutathione thiyl ($GS^{\bullet\bullet}$) biradical. The optimized structure of the product obtained from this reaction is shown in Figure S4. This reduction occurs in a barrierless reaction in the gas and aqueous media. Thus, glutathione is converted into the $GS^{\bullet\bullet}$ biradical. It has been shown in earlier studies that the presence of $GS^{\bullet\bullet}$ will affect the function of other antioxidant enzymes present in the biological systems.[54] In the lipid phase, the H atom abstraction from the carboxylic acid group is found to take place without any barrier, but the reaction corresponding to H atom abstraction in the second step is not observed. This is due to the high concentration of unsaturated fatty acids present in lipid medium which excludes the reaction with the S atom of the key antioxidant molecules. The calculated Gibb's free energy of the reaction is −23.02, −32.52, and −38.71 kcal/mol respectively in gas, aqueous, and lipid phases.

B. Thermochemical Properties. The Gibbs free energy of activation, ΔG^{act}, and the entropy of activation, ΔS^{act}, of the intermediates and products in the three phases are summarized in Table 3. The free energy of activation in solvent medium is calculated by including the solvent cage effect. The major

Table 3. Calculated Thermochemical Properties, Enthalpy (ΔH in kcal/mol), Change in Entropy (ΔS in cal K/mol), and Gibbs Free Energy (ΔG in kcal/mol) of the Studied Reactions[a]

	gas				aqueous				lipid			
reactive species	ΔH	ΔS	$\Delta S^{act}_{gas,calc}$	ΔG	$\Delta G^{act}_{gas,calc}$	ΔH	ΔS	$\Delta S^{act}_{aqu,calc}$	ΔG	$\Delta G^{act}_{aqu,calc}$	ΔH	ΔS	$\Delta S^{act}_{lip,calc}$	ΔG	$\Delta G^{act}_{lip,calc}$
I1	−32.6	−5.7	−10.3	−34.3	29.3	−6.6	−12.1	−22.4	−30.8	33.6	−37.4	−14.9	−19.7	−32.9	52.6
I2	−30.2	−0.04	−20.2	−26.7	28.7	−34.3	−12.2	−32.4	−3.3	155.2	−31.8	−11.3	−32.2	−28.4	161.5
I3	0.1	−14.0	−15.4	4.3	18.2	2.5	−13.1	−28.4	5.8	36.3	0.2	−12.8	−34.1	4.1	51.0
I4	−62.8	−5.0	−15.3	−61.3	8.7	−65.0	−16.8	−32.1	−64.0	43.3	−62.2	−5.5	−25.2	−60.6	41.5
I5	−1.5	−9.7	−11.7	1.3	24.2	−0.8	−13.2	−24.9	1.9	28.9	17.2	−10.9	−29.3	20.4	31.0
I6	−50.0	−9.8	−19.5	−47.1	1.3	−65.2	−12.4	−32.0	−63.4	6.7	−59.7	−5.9	−33.2	−58.0	17.1
P1	0.2	−0.04	−2.2	0.3	9.5	−2.2	−1.6	−6.1	−4.7	7.7	−3.1	−1.5	−1.9	−2.7	11.6
P2	−15.9	−16.1	−3.4	−11.1	−9.5	−18.4	−19.0	−5.6	−15.7	−12.3	−17.2	−17.5	−8.8	−12.0	−10.8
P3	−13.2	−12.2	−16.5	−16.9	20.2	0.001	−0.04	−31.9	−2.9	20.2	19.1	−8.3	−15.6	−21.5	44.7
P4	23.3	12.7	−0.02	−27.1	2.9	23.9	−8.9	−9.5	23.6	32.8	23.1	−11.2	−12.7	26.5	33.1
P5	−7.4	6.1	−15.3	−9.2	78.1	−10.6	10.5	−22.7	−16.6	70.1	−10.3	10.0	−11.1	−13.3	61.8
P6	−22.6	−2.9	−5.1	−21.8	23.1	−21.6	−3.9	−9.7	−23.4	21.1	−23.6	−2.2	−12.4	−22.9	8.9

[a] $\Delta G^{act}_{aq,calc} = \Delta G^{act}_{gas,calc} + \Delta G^{act}_{solv,calc}$; $\Delta S^{act}_{aq,calc} = \Delta S^{act}_{gas,calc} + \Delta S^{act}_{solv,calc}$; $\Delta H_{aq} = \Delta H_{prod(aq)} - \Delta H_{react(aq)}$.

dx.doi.org/10.1021/jp4106037 | J. Phys. Chem. B 2014, 118, 3479−3490

Table 4. Rate Constants (k in cm^3 molecule^{-1} s^{-1}) for the Formation of the Intermediates I1 and I3 and Products P1 and P3

	k_{I1}	k_{P1}	k_{I3}			k_{P3}		
temp (K)	aqueous ($\times 10^{-11}$)	aqueous ($\times 10^{-17}$)	gas ($\times 10^{-14}$)	aqueous ($\times 10^{-16}$)	lipid ($\times 10^{-15}$)	gas ($\times 10^{-18}$)	aqueous ($\times 10^{-19}$)	lipid ($\times 10^{-14}$)
278	0.006	1.06	5.37	3.95	1.8	2.32	7.56	3.44
288	0.03	1.60	6.65	5.06	2.45	3.67	8.45	4.78
298	0.12	2.37	8.13	6.34	3.28	5.72	9.72	5.55
308	0.45	3.44	9.83	7.85	4.33	8.35	11.74	7.76
318	1.58	4.88	11.76	9.61	5.62	10.13	13.67	8.23
328	5.14	6.78	13.94	11.66	7.19	11.87	15.11	9.35
338	15.61	9.28	16.37	14.02	9.09	13.54	18.75	11.43
348	44.32	12.56	19.08	16.71	11.36	17.33	21.32	13.44
350	54.21	13.24	19.65	17.3	11.86	19.21	23.11	15.67
						20.0	23.86	16.01

entropic contribution is from the cavity formation which is originated from the change in solvent structure.[29] It is observed from Table 3 that the entropic contribution to free energy of activation is significant for most of the intermediates, and the activation entropy of the species calculated in the solvent phase is larger than that in the gas phase. The negative entropy of activation indicates the hydrogen bonding and other attractive interactions between the polar functional groups of tyrosine and solvent molecules. The solvation increases the entropy of activation for tyrosine−O_3 adduct reactions (**I4**, **I5**, and **I6**) due to the neutralization of the products which have no reactive sites for further interaction with the solvent molecules. The Gibbs free energy of activation is larger in the solvent media which is due to the large contribution of entropy of activation to Gibbs free energy.

The enthalpy (ΔH) and the Gibbs free energy of the reaction (ΔG) at 298.15 K for initial oxidation and the subsequent nitration reactions are summarized in Table 3 for both gas and solvent media. The calculated ΔH values show that all the studied reactions are exothermic, except the formation of **I3** which occurs in a mild endothermic reaction. The largest exothermicity is observed for the formation of intermediate **I4**. The calculated ΔG values show that the formation of intermediate **I4** is highly exoergic with ΔG value of −61.3, −60.6, and −64.0 kcal/mol respectively in gas, lipid, and aqueous media. The Gibbs free energy for the formation of intermediate **I5** shows that the reaction is slightly endoergic in gas and aqueous media, but in lipid media the reaction is highly endoergic. Such influence of the lipid medium is due to the strong stabilizing effect of the solvent toward the C-centered radical formed after O_3 addition. The enthalpy and free energy of the reactions show that the formation of the 3-hydroxytyrosine, **I4**, is kinetically favorable. But, the subsequent nitration of **I4** is less favorable with an endothermicity of 23.3, 23.9, and 23.2 kcal/mol in gas, aqueous, and lipid phases, respectively. This is due to the presence of OH group at the para position of tyrosine. The nitrotyrosine (**P1**) product channel is formed with least endoergicity of 0.2 kcal/mol in gas phase and with a mild exoergicity of −4.7 and −2.7 kcal/mol respectively in aqueous and lipid media. This result and the calculated energy barrier show that the formation of P1 product channel is both thermodynamically and kinetically favorable in the aqueous medium. The kinetically favorable nitration reaction is the formation of product **P4** in gas phase, whereas in the solvent media, the formation of product channel **P6** is kinetically favorable.

C. Kinetics. From the potential energy surface characterization of the reactive species, it is observed that the intermediate **I1** is formed more favorably in aqueous medium and the formation of intermediate **I3** is equally favorable in all the three media studied. Hence, the rate constant is calculated for the intermediate **I1** and its subsequent nitrated product **P1** in aqueous medium and the intermediate **I3** and the subsequent nitration product **P3** in all the three media. The rate constants k_{I1}, k_{P1}, k_{I3}, and k_{P3} for the intermediate **I1**, product **P1**, intermediate **I3**, and product **P3**, respectively, are calculated over the temperature range of 278−350 K and are summarized in Table 4. The intermediate **I1** is formed more rapidly in the aqueous medium with a rate constant of 0.12×10^{-12} cm^3 molecule^{-1} s^{-1} at 298 K. The tunneling factor is negligible in this initial reaction. The variational transition state corresponding to this reaction is located at s = 0.01 Å. The product **P1** is formed with a rate constant of 2.37×10^{-17} cm^3 molecule^{-1} s^{-1} at 298 K. The tunneling factor for this reaction is appreciable with a transmission coefficient of 4.2. The variational transition state involved in the product **P1** formation is located at the reaction coordinate, s = −0.001 Å. Consistent with the energetic analysis, the formation of intermediate **I3** occurs comparably faster in the gas phase than in the solvent media. Over the whole temperature range studied, the rate constant calculated in the solvent media is about 1−2 orders of magnitude smaller than that in the gas phase. As expected, the tunneling factor in the solvent media is higher by 2 orders of magnitude than in the gas phase. The variational correction for the initial reaction is negligible in all the three media. The variational transition state involved in the formation of **I3** intermediate is located at the reaction coordinate, s = −0.0004, 0.0007, and 0.0002 Å, respectively in gas, aqueous, and lipid media. The calculated rate constant for the initial oxidation reveals that the formation of tyrosine radical is irreversible under atmospheric conditions. This observation is in agreement with the earlier result that the atmospheric oxidants can cause irreversible damage to biomolecules.[49] The large magnitude of the rate constant in gas phase show that the oxidation of tyrosine is faster in gas phase, thereby acting as a sink for atmospheric ozone. As given in Table 4, the rate constant k_{P3} calculated for the **P3** product channel shows that the nitration occurs comparatively faster in the lipid medium. This result shows that the nitration is thermodynamically favorable in nonpolar solvents. The tunneling effect is negligible in this reaction. The variational correction for this reaction is 2.5 over the whole temperature range studied. The variational transition state for this reaction is located at the reaction coordinate s = −0.002, −0.12, and 0.023 Å respectively in gas, aqueous, and lipid media. The lower magnitude of the rate constant calculated for this nitration reveal that the pK_a value of the

dx.doi.org/10.1021/jp4106037 | J. Phys. Chem. B 2014, 118, 3479−3490

carboxylic acid group of tyrosine is an important factor in controlling the nitration in aqueous phase, whereas in lipid medium, the pentyl ethanoate solvent is a better electron donor and influence the nitration. The pK_a value for the carboxylic acid group of tyrosine is 1.93. This value compares quite well with the experimental pK_a value of 2.09. Thus, the rate of oxidation and nitration depends on the medium, and under ambient atmospheric conditions in polluted air, the rate of formation of the intermediate **I3** is faster. On comparing the rate constant for the initial oxidation reactions in aqueous medium, the intermediate **I1** is formed faster than the intermediate **I3**. Also, the nitrated product **P1** is formed comparably with a faster rate than the product **P3** in aqueous medium. These results reveal that the formation of intermediate **I1** and its subsequent nitrated product **P1** is more favorable in aqueous medium, while in the other two media studied, the formation of the intermediate **I3** and its nitrated product **P3** is more favorable.

D. Spectral Properties. The spectral properties of tyrosine, intermediates **I1** and **I3**, and their nitrated products **P1** and **P3** are studied using the TDDFT-M06-2X/6-311+G(d,p) level of theory. The absorption and CD spectra of the free tyrosine, intermediate **I1** and product **P1**, and intermediate **I3** and the product **P3** are given in Tables S4−S6. As given in Tables S4−S6, the spectra of tyrosine, its oxidation and nitration products vary significantly in the three phases. This is attributed to the solvent cage effect which results from a mechanical restriction on intramolecular conformational changes of the molecule upon electronic excitation. In such cases, a shift in the band origin is observed and the vibrational distribution pattern will change.[55] In the gas phase spectra of tyrosine, the more intense band is observed around 213 nm, whereas in the aqueous medium, the most intense band is observed at 184 nm and in the lipid medium, the more intense band appears at 186 nm. This absorption band corresponds to $\pi \rightarrow \pi^*$ transition. As observed from Table S4, a high intensity positive Cotton effect is predicted at 185 and 190 nm, respectively, in the aqueous and lipid phases, whereas in the gas phase no intense positive signal is noted in the CD spectra.

As given in Table S5, the spectra of the tyrosyl radical **I1** show long wavelength shift from that of the tyrosine. In this case, the intense absorption band is noted at 234 nm in gas phase and around 286 and 377 nm in aqueous and lipid phases, respectively. The low intensity absorption at wavelength >250 nm is more solvent-sensitive than the band envelope as a whole. The most intense 234 nm band in gas phase is not perceivable in the solvent phases, and this results in the red-shift of a very intense $\pi \rightarrow \pi^*$ band. In solvent medium, there is no distinct band in the CD spectra of the tyrosyl radical compared to the absorption spectra of tyrosine. In the gas phase, a large positive and negative Cotton effect is predicted at 600 and 420 nm, respectively. This is because the rotational strength of the $\pi \rightarrow \pi^*$ band is affected upon solvation, and the $\pi \rightarrow \pi^*$ transitions tend to couple with the neighboring amino acid residues. An internal hydrogen bond exists between the nitro group and OH group of nitrotyrosine (**P1**). This makes the absorption properties to be strongly pH-dependent.[56] The nitrotyrosine have distinct spectra with an intense band at about 210 nm in gas phase, whereas in the aqueous and lipid phases, the most intense band is predicted at 256 and 212 nm, respectively. The calculated red-shift in the aqueous medium is attributed to the change in dipole moment orientation with respect to the dipolar orientation of the surrounding polar medium. The maximum absorbance at 276 nm is common to all aromatic amino acids.[56] Further, the large absorbance red-shift is due to the high dielectric constant of the water solvent. The more intense band in tyrosine remains the same in nitrotyrosine in gas phase, whereas in the solvent phases, the more intense absorption band is shifted toward longer wavelength region. This is because in the solvent media, the nitrotyrosine becomes more hydrophilic than tyrosine. In addition to this effect, the steric hindrance in nitrotyrosine also changes the characteristic spectra. The CD spectra of the **P1** is maximum at 202, 230, and 240 nm in gas, aqueous, and lipid phases, respectively, and the spectra in aqueous and lipid phases show a zero-crossing at 260 nm (see Table S5). The negative Cotton effect is predicted at 198 nm in gas phase, while in lipid phase, at 198 nm a positive Cotton effect is predicted. As expected, beyond 290 nm, the Cotton effect approaches zero. These results show that the environment directly influences the computed transition properties.

As given in Table S6, in the spectra of the **I3** complex, the most intense absorption bands appear at 214, 195, and 297 nm respectively in gas, aqueous, and lipid media. That is, the UV absorption band of the **I3** complex shifts toward the shorter wavelengths in polar solvent. In this case, the calculated blue-shift is due to decrease in dipole moment upon excitation in which the ground state of the **I3** complex in aqueous phase will lie lower in energy than the corresponding excited state. This blue-shift is blocked by the solvent cage when the medium is lipid and hence the most intense absorption band of the **I3** complex is red-shifted in the lipid medium. During the complex formation in lipid milieu, the more intense band of tyrosine is red-shifted by about 110 nm in the **I3** complex. The CD spectra of the **I3** complex show dichroism in the weak band regions. This may be due to the transition involved in an apparent Cotton effect observed in the optical rotatory dispersion of the **I3** complex. The more intense absorption band in the spectra of the **P3** complex is observed at 275, 287, and 287 nm respectively in gas, aqueous, and lipid phases (see Table S6). Thus, in solvent phase, a slight red-shift in the absorption band is observed. The solvent cage restricts the change of dipole moment orientation in the excited state from that of the ground state which leads to red-shift in absorption band in solvent medium. Upon going from tyrosine to **P3** form, the more intense band of tyrosine becomes much more intense and the $\pi \rightarrow \pi^*$ transition is split into a couplet, leading to a shoulder at 287 nm in gas phase. The CD spectra for the **P3** form in both the solvents show similar couplet for the $\pi \rightarrow \pi^*$ transition, but with higher intensities than the gas phase. These findings suggest that both the nitrated forms of tyrosine possess optical activity under different pH conditions. That is, the **P3** nitrated form of tyrosine possess similar biological implications as reported for **P1** form in earlier studies,[12] and a qualitative understanding of the **P3** nitrated form is essential to improve the air quality and control the allergy-related diseases.

CONCLUSIONS

The theoretical results reported in this study present an elucidation of the reaction mechanism and pathways involved in the nitration of tyrosine by the atmospheric oxidants, O_3 and NO_2 in the gas, aqueous and lipid media. From the analysis of the results, we arrive at the following main conclusions:

1. The reaction between tyrosine and O_3 proceeds by H atom abstraction and addition reactions leading to the

dx.doi.org/10.1021/jp4106037 | J. Phys. Chem. B 2014, 118, 3479−3490

formation of six intermediates. Of all the intermediates studied, the intermediate **I3** in which a tyrosine radical is formed is found to be the most favorable with a small energy barrier in all the three phases studied.

2. The tyrosyl radical **I1** observed in the earlier experimental studies is found to be the rate determining intermediate in the initial oxidation reaction in gas and lipid media. In aqueous media, the formation of the tyrosyl radical (**I1**) occurs with a small energy barrier of 3.88 kcal/mol.
3. The tyrosyl radical is stabilized through self-reaction resulting in the formation of tyrosine dimer. This dimerization reaction occurs favorably in gas and aqueous media with energy barrier of 35.56 and 21.23 kcal/mol, respectively, whereas the reaction is less feasible in the lipid medium. This dimer alters the protein assembly and assists protein degradation.
4. The subsequent nitration reaction is studied for all the intermediates in the three media. The results show that the nitration affects both the side chain as well as the aromatic ring of tyrosine. The formation of nitrotyrosine, **P1**, occurs more feasibly in the aqueous media, and the nitrated form of tyrosine, **P3**, resulting from the nitration of tyrosine radical, **I3**, occurs more favorably in the gas phase.
5. The fate of the tyrosine radical, **I3**, is determined by its reaction with an antioxidant glutathione. The reaction regenerated the tyrosine in a barrierless reaction, along with a glutathione thiyl radical. The conversion of glutathione into glutathione biradical causes inability of the living organisms to resist stress.
6. The tyrosine radical is formed more favorably than the tyrosyl radical and possesses significant biological implications as the tyrosyl radical. Hence, it is very important to analyze through experimental studies whether the formation of **P3** product channel is a general feature observed in a wide range of inflammatory immune responses, which is responsible for oxidative stress.
7. The results of this study clearly demonstrate that tyrosine is efficiently nitrated by O_3 and NO_2 present in polluted air. The study provides a molecular rationale for understanding the atmospheric chemistry behind the nitration process in the context of supporting the hypothesis that protein nitration by polluted air may induce the allergic diseases.

■ ASSOCIATED CONTENT

Supporting Information

Energy barrier calculated at the M06-2X/6-31G(d,p) level of theory is summarized in Table S1; energy barrier calculated at the B3LYP and B3LYP-D methods with 6-311+G(d,p) level of theory is given in Table S2; total energies of the reactive species optimized at the M06-2X/6-311+G(d,p) level of theory in gas, aqueous, and lipid media are summarized in Table S3; absorption and CD spectra of the free tyrosine, intermediate **I1** and product **P1**, and intermediate **I3** and product **P3** are given in Tables S4−S6; optimized structure of the intermediates and products formed in the initial oxidation and subsequent nitration reactions is illustrated in Figure S1; optimized structure of the transition state and the product corresponding to the nitration reaction of tyrosyl radical, **I1**, is given in Figure S2; optimized structure of the tyrosine dimer and the tyrosine + glutathione thiyl radical product channel is shown in Figures S3 and S4, respectively; optimized Cartesian coordinates (in Å) of the reactive species in the three media studied are given. This material is available free of charge via the Internet at http://pubs.acs.org.

■ AUTHOR INFORMATION

Corresponding Author

*Fax +91-422-2422387, e-mail ksenthil@buc.edu.in (K.S.).

Notes

The authors declare no competing financial interest.

■ ACKNOWLEDGMENTS

L.S. is thankful to the Department of Science and Technology (DST), Govt. of India, for awarding INSPIRE Fellowship. K.S. is thankful to the University Grants Commission (UGC), Govt. of India, for granting major research project. The authors thank the reviewers for giving valuable suggestions to improve the manuscript.

■ REFERENCES

(1) Finlayson-Pitts, B. J.; Pitts, J. N. Tropospheric Air Pollution: Ozone, Airborne Toxics, Polycyclic Aromatic Hydrocarbons, and Particles. *Science* **1997**, *276*, 1045.

(2) Finlayson-Pitts, B. J.; Pitts, J. N. *Chemistry of the Upper and Lower Atmosphere*; Academic Press: San Diego, 2000.

(3) Poschl, U. Atmospheric Aerosols: Composition, Transformation, Climate and Health Effects. *Angew. Chem., Int. Ed.* **2005**, *44*, 7520.

(4) D'Amato, G.; Liccardi, G.; D'Amato, M.; Cazzola, M. The Role of Outdoor Air Pollution and Climatic Changes on the Rising Trends in Respiratory Allergy. *Respir. Med.* **2001**, *95*, 606.

(5) Knox, R. B.; Suphioglu, C.; Taylor, P.; Desai, R.; Watson, H.-C.; Peng, J. L.; Bursill, L. A. Major Grass Pollen Allergen Lol p 1 Binds to Diesel Exhaust Particles: Implications for Asthma and Air Pollution. *Clin. Exp. Allergy* **1997**, *27*, 246.

(6) Samet, J.; Wassel, R.; Holmes, K. J.; Abt, E.; Bakshi, K. Research Priorities for Airborne Particulate Matter in the United States. *Environ. Sci. Technol.* **2005**, *39*, 299A.

(7) Brunekreef, B. NO_2: The Gas That Won't Go Away. *Clin. Exp. Allergy* **2001**, *31*, 1170.

(8) Ring, J.; Eberlein-Koenig, B.; Behrendt, H. Environmental Pollution and Allergy. *Ann. Allergy Asthma Immunol.* **2001**, *87*, 2.

(9) Franze, T.; Weller, M. G.; Niessner, R.; Poschl, U. Protein Nitration by Polluted Air. *Environ. Sci. Technol.* **2005**, *39*, 1673.

(10) Shiraiwa, M.; Sosedova, Y.; Rouviere, A.; Yang, H.; Zhang, Y.; Abbatt, J. P.; Ammann, M.; Poschl, U. The Role of Long-lived Reactive Oxygen Intermediates in the Reaction of Ozone with Aerosol Particles. *Nat. Chem.* **2011**, *3*, 291.

(11) Hakim, M.; Broza, Y. Y.; Barash, O.; Peled, N.; Phillips, M.; Amann, A.; Haick, H. Volatile Organic Compounds of Lung Cancer and Possible Biochemical Pathways. *Chem. Rev.* **2012**, *112*, 5949.

(12) Radi, R. Protein Tyrosine Nitration: Biochemical Mechanisms and Structural Basis of Functional Effects. *Acc. Chem. Res.* **2013**, *46*, 550.

(13) Diaz-Moreno, I.; Nieto, P. M.; Del Conte, R.; Gairi, M.; Garcia-Heredia, J. M.; De la Rosa, M. A.; Diaz-Quintana, A. A Non-Damaging Method to Analyze the Configuration and Dynamics of Nitrotyrosines in Proteins. *Chem.—Eur. J.* **2012**, *18*, 3872.

(14) Souza, J. M.; Peluffo, G.; Radi, R. Protein Tyrosine Nitration-Functional Alteration orJust a Biomarker? *Free Radicals Biol. Med.* **2008**, *45*, 357.

(15) Radi, R. Nitric Oxide, Oxidants, and Protein Tyrosine Nitration. *Proc. Natl. Acad. Sci. U. S. A.* **2004**, *101*, 4003.

(16) Bartesaghi, S.; Valez, V.; Trujillo, M.; Peluffo, G.; Romero, N.; Zhang, H.; Kalyanaraman, B.; Radi, R. Mechanistic Studies of

Peroxynitrite-Mediated Tyrosine Nitration in Nembranes Using the Hydrophobic Probe N-t-BOC-L-Tyrosine Tert-Butyl Ester. *Biochemistry* **2006**, *45*, 6813.
(17) Bartesaghi, S.; Wenzel, J.; Trujillo, M.; Lopez, M.; Joseph, J.; Kalyanaraman, B.; Radi, R. Lipid Peroxyl Radicals Mediate Tyrosine Dimerization and Nitration in Membranes. *Chem. Res. Toxicol.* **2010**, *23*, 821.
(18) Shiraiwa, M.; Selzle, K.; Yang, H.; Sosedova, Y.; Ammann, M.; Poschl, U. Multiphase Chemical Kinetics of the Nitration of Aerosolized Protein by Ozone and Nitrogen dioxide. *Environ. Sci. Technol.* **2012**, *46*, 6672.
(19) Prutz, W. A.; Monig, H.; Butler, J.; Land, E. J. Reactions of Nitrogen Nioxide in Aqueous Model Systems: Oxidation of Tyrosine Units in Peptides and Proteins. *Arch. Biochem. Biophys.* **1985**, *243*, 125.
(20) Eiserich, J. P.; Butler, J.; van der Vliet, A.; Cross, C. E.; Halliwell, B. Nitric Oxide Rapidly Scavenges Tyrosine and Tryptophan radicals. *Biochem. J.* **1995**, *310*, 745.
(21) Buettner, G. R. The Pecking Order of Free Radicals and Antioxidants. Lipid Peroxidation, a-Tocopherol, and Ascorbate. *Arch. Biochem. Biophys.* **1993**, *300*, 535.
(22) Winterbourn, C. C. Superoxide as an Intracellular Radical Sink. *Free Radicals Biol. Med.* **1993**, *14*, 85.
(23) Gebicki, J. M.; Nauser, T.; Domazou, A.; Steinmann, D.; Bounds, P. L.; Koppenol, W. H. Reduction of Protein Radicals by GSH and Ascorbate: Potential Biological Significance. *Amino Acids* **2010**, *39*, 1131.
(24) Zhao, Y.; Truhlar, D. G. The M06 Suite of Density Functionals for Main Group Thermochemistry, Thermochemical Kinetics, Noncovalent Interactions, Excited States, and Transition Elements: Two New Functionals and Systematic Testing of Four M06-class Functionals and 12 Other Functionals. *Theor. Chem. Acc.* **2008**, *120*, 215.
(25) Zhao, Y.; Truhlar, D. G. Density Functionals with Broad Applicability in Chemistry. *Acc. Chem. Res.* **2008**, *41*, 157.
(26) Luo, S.; Zhao, Y.; Truhlar, D. G. Validation of Electronic Structure Methods for Isomerization Reactions of Large Organic Molecules. *Phys. Chem. Chem. Phys.* **2011**, *13*, 13683.
(27) Zheng, J.; Zhao, Y.; Truhlar, D. G. The DBH24/08 Database and Its Use to Assess Electronic Structure Model Chemistries for Chemical Reaction Barrier Heights. *J. Chem. Theory Comput.* **2009**, *5*, 808.
(28) Xu, X.; Alecu, I. M.; Truhlar, D. G. How Well Can Modern Density Functionals Predict Intermolecular Distances at Transition State. *J. Chem. Theory Comput.* **2011**, *7*, 1667.
(29) Marenich, A. V.; Cramer, C. J.; Truhlar, D. G. Universal Solvation Model Based on Solute Electron Density and on a Continuum Model of the Solvent Defined by the Bulk Dielectric Constant and Atomic Surface Tensions. *J. Phys. Chem. B* **2009**, *113*, 6378.
(30) Assary, R. S.; Redfern, P. C.; Greeley, J.; Curtiss, L. A. Mechanistic Insights into the Decomposition of Fructose to Hydroxy Methyl Furfural in Neutral and Acidic Environments Using High-Level Quantum Chemical Methods. *J. Phys. Chem. B* **2011**, *115*, 4341.
(31) Assary, R. S.; Curtiss, L. A. A Comparison of Sugar Molecule Decomposition through Glucose and Fructose: A High Level Quantum Chemical Study. *Energy Fuels* **2012**, *26*, 1344.
(32) Benson, S. W. In *The Foundation of Chemical Kinetics*; Robert, E., Ed.; Krieger: Malabar, FL, 1982.
(33) Okuno, Y. Theoretical Investigation of the Mechanism of the Baeyer-Villiger Reaction in Nonpolar Solvents. *Chem.—Eur. J.* **1997**, *3*, 210.
(34) Valero, R.; Andersson, S. Quantitative Integral Cross Sections for the H + CO_2 → OH + CO Reaction from a Density Functional Theory-Based Potential Energy Surface. *Phys. Chem. Chem. Phys.* **2012**, *14*, 16699.
(35) Pople, J. A.; Head-Gordon, M.; Raghavachari, K. Quadratic Configuration Interaction. A General Technique for Determining Electron Correlation Energies. *J. Chem. Phys.* **1987**, *87*, 5968.
(36) Becke, A. D. Density-Functional Thermochemistry. III. The Role of Exact Exchange. *J. Chem. Phys.* **1993**, *98*, 5648.
(37) Grimme, S. Semiempirical GGA-type Density Functional Constructed with a Long-Range Dispersion Correction. *J. Comput. Chem.* **2006**, *27*, 1787.
(38) Wu, Q.; Yang, W. Empirical Correction to Density Functional Theory for van der Waals Interactions. *J. Chem. Phys.* **2002**, *116*, 515.
(39) Cossi, M.; Baroni, V. Time-Dependent Density Functional Theory for Molecules in Liquid Solutions. *J. Chem. Phys.* **2001**, *115*, 4708.
(40) Diedrich, C.; Grimme, S. Systematic Investigation of Modern Quantum Chemical Methods to Predict Electronic Circular Dichroism Spectra. *J. Phys. Chem. A* **2003**, *107*, 2524.
(41) Frisch, M. J.; Trucks, G. W.; Schlegel, H. B.; Scuseria, G. E.; Robb, M. A.; Cheeseman, J. R.; Scalmani, G.; Barone, V.; Mennucci, B.; Petersson, G. A. et al. Gaussian, Inc., Wallingford, CT, 2009.
(42) Zheng, J.; Zhang, S.; Corchado, J. C.; Chuang, Y. Y.; Coitino, E. L.; Ellingson, B. A.; Truhlar, D. G. *GAUSSRATE version*, 2009.
(43) Zheng, J.; Zhang, S.; Lynch, B. J.; Corchado, J. C.; Chaung, Y. Y.; Fast, P. L.; Hu, W. P.; Liu, Y. P.; Lynch, G. C. et al. *POLYRATE version*, 2010.
(44) Jackson, P.; Beste, A.; Attalla, M. I. CO_2 Capture in Aqueous Ammonia Solutions: A Computational Chemistry Perspective. *Phys. Chem. Chem. Phys.* **2012**, *14*, 16301.
(45) Koide, S.; Sidhu, S. S. The Importance of Being Tyrosine: Lessons in Molecular Recognition from Minimalist Synthetic Binding Proteins. *ACS Chem. Biol.* **2009**, *4*, 325.
(46) Harrison, M. A. J.; Barra, S.; Borghesi, D.; Vione, D.; Arsene, C.; Olariu, R. L. Nitrated Phenols in the Atmosphere: A Review. *Atmos. Environ.* **2005**, *39*, 231.
(47) Sosedova, Y.; Rouviere, A.; Bartels-Rausch, T.; Ammann, M. UVA/Vis-Induced Nitrous Acid Formation on Polyphenolic Films Exposed to Gaseous NO_2. *Photochem. Photobiol. Sci.* **2011**, *10*, 1680.
(48) Yokoyama, H.; Uhlin, U.; Stubbe, J. Site-Specific Incorporation of 3-Nitrotyrosine as a Probe of pKa Perturbation of Redox-Active Tyrosines in Ribonucleotide Reductase. *J. Am. Chem. Soc.* **2010**, *132*, 8385.
(49) Goeschen, C.; Wibowo, N.; White, J. M.; Wille, U. Damage of Aromatic Amino Acids by the Atmospheric Free Radical Oxidant NO_3 in the Presence of NO_2, N_2O_4, O_3 and O_2. *Org. Biomol. Chem.* **2011**, *9*, 3380.
(50) Bartesaghi, S.; Ferrer-Sueta, G.; Peluffo, G.; Valez, V.; Zhang, H.; Kalyanaraman, B.; Radi, R. Protein Tyrosine Nitration in Hydrophilic and Hydrophobic Environments. *Amino Acids* **2007**, *32*, 501.
(51) Santos, C. X.; Bonini, M. G.; Augusto, O. Role of the Carbonate Radical Anion in Tyrosine Nitration and Hydroxylation by Peroxynitrite. *Arch. Biochem. Biophys.* **2000**, *377*, 146.
(52) Sosedova, Y.; Rouviere, A.; Gaggeler, H. W.; Ammann, M. Uptake of NO_2 to Deliquesced Dihydroxybenzoate Aerosol Particles. *J. Phys. Chem. A* **2009**, *113*, 10979.
(53) Pattison, D. I.; Rahmanto, A. S.; Davies, M. J. Photo-oxidation of Proteins. *Photochem. Photobiol. Sci.* **2012**, *11*, 38.
(54) Rahmanto, A. S.; Morgan, P. E.; Hawkins, C. L.; Davies, M. J. Cellular Effects of Peptide and Protein Hydroperoxides. *Free Radicals Biol. Med.* **2010**, *48*, 1071.
(55) Dellinger, B.; Kasha, M. Intermolecular Perturbation of Molecular Potentials. *Chem. Phys. Lett.* **1975**, *36*, 410.
(56) De Filippis, V.; Frasson, R.; Fontana, A. 3-Nitrotyrosine as a Spectroscopic Probe for Investigating Protein Protein Interactions. *Protein Sci.* **2006**, *15*, 976.